International Conference on Intelligent Technologies & Science - 2021
(ICITS-2021)

Evaluation of Mechanical and Metallurgical Properties of MgO added Al_2O_3/ZrO_2 Ceremics

Alok Ranjan Yadav[1], Dr. Bipin Kumar Singh[2]
Mechanical Engineering,
Goel Institute of Technology & Management, Lucknow, India
aryayadu@rocketmail.com, bipinmech1986@gmail.com

Abstract: In streaming nitrogen, non-oxides, for example, Al4O4C, Al2OC, Zr2Al3C4, and MgAlON reinforced Al2O3-based composites were effectively ready by a vaporous stage mass exchange pathway utilizing aluminum, zirconia, alumina, and magnesia as crude materials at 1873 K, after an Al–AlN center shell structure was shaped at 853 K. Gum reinforced Al–Al2O3–MgO–ZrO2 composites subsequent to sintering were described and examined by X-beam diffraction (XRD), filtering electron magnifying lens (SEM) and, energy dispersive spectrometer (EDS), and the impact of the MgO content on the sintered composites was considered. The outcomes show that in the wake of sintering, the stage structure of the Al–Al2O3–ZrO2 composite is Al2O3, Al4 O4C, Al2OC, and Zr2Al3C4, while the stage sythesis of the Al–Al2O3–ZrO2 composite with the expansion of MgO 6 wt% and MgO 12 wt% is Al2O3, MgAlON, Al4O4C, Al2OC, and Zr2Al3C4 just as Al2O3, MgAlON, Al2OC, and Zr2Al3C4, separately. The expansion of MgO changed the stage creation and conveyance for the pitch fortified Al–Al2O3–MgO–ZrO2 framework composites in the wake of sintering. When the additional MgO content is equivalent to or more than 12 wt%, the Al4O4C in the tar reinforced Al–Al2O3–MgO–ZrO2 framework composites can't exist in a steady stage.

Keywords: Cutting inserts, MgO, Particle size, ZTA, Wear performance

1. Introduction

Alumina-zirconia-carbon (Al2O3–ZrO2–C) refractories have been broadly utilized in the steel business, for example, in plugs, sliding plates, or lowered spouts, attributable to their great warm shock opposition, phenomenal slag erosion obstruction, and low coefficient of warm expansion.1,2 To further develop the oxidation obstruction and mechanical strength of carbon-containing refractories, cancer prevention agents are frequently

added. Of these cancer prevention agents, Al is frequently brought into Al2O3–ZrO2–C refractories as antioxidants,3,4 in which non-oxides with elite, for example, Al4O4C, Al2OC, Zr2Al3C5, and AlON are created by the solid decrease movement of aluminum at high temperatures, working on the physical and compound properties of the recalcitrant. Nonetheless, with the improvement of refining innovation, for example, clean steel and low-carbon steel, refractories with low carbon content are required.5,6 It is notable that the decreased carbon content of Al2O3–ZrO2-C refractories will break down its application exhibitions, like its great warm shock obstruction and astounding slag erosion opposition, to additionally debilitate its administration life. Consequently, on account of lower levels or missing graphite and carbon dark (just pitch existing as a holding specialist 8), the turn of events and readiness of Al2O3–ZrO2–C refractories with astounding exhibitions is a flow research accentuation. Non-oxides, like Al4O4C, Al2OC, Zr2Al3C4, and AlON, have high warm conductivity, great warm shock opposition, a low wetting point to fluid steel, a hydration obstruction better than Al4C3, and oxidation obstruction obviously superior to graphite and carbon black.9-18 Thus, non-oxide, instead of oxide composites, have been a flow standard heading in the headstrong field. Al4O4C and Al2OC are incongruent-liquefying compounds in the Al4C3–Al2O3 twofold framework with disintegration temperatures that are ~2143 and 2263 K, respectively.19-25 Al4O4C can be shaped at 1473 K and higher temperatures, and Al2OC can't be framed and decayed into Al4O4C and Al4C3 with hydration trademark under 1988 K, as indicated by the response 4Al2CO(s) ! Al4O4C(s) þ Al4 C3(s).21 Both AlN and Al2CO have the hexagonal wurtzite structure, so Al2CO can be settled by the disintegration of modest quantities of AlN into Al2OC to forestall its deterioration reaction.25 Zr2Al3C4, which comprises of elective piles of NaCl-type Zr–C chunks and Al4C3-type Al–C units, was for the most part ready at high temperatures utilizing Zr/ZrC, Al, and graphite powders as the beginning materials.11-15,26,27 The costs of Zr/ZrC and their creation costs are high, which restricts their mechanical application. AlON is a spinel strong arrangement with changed organization in an AlN–Al2O3 paired framework and can't be balanced out beneath 1640°C, 10°C.28-30 It has been shown that AlON can be settled underneath this temperature through the expansion of MgO and MgAl2O4 as a strong arrangement spinel stage, signified as MgAlON.30 The dissolving point of aluminum is 933 K, and its fluid thickness (0.104 Pas) is near that of water at 293 K (0.10 Pas). The low consistency of fluid aluminum can block its nitridation and carbothermal responses, further bringing about inhomogeneity of the response item and debilitating application properties at high temperatures. Not quite the same as fluid and strong mass exchange, the response result of gas mass exchange has super-high surface energy and

response energy, which can speed up the response cycle, further develop the dissemination consistency of the response item, and upgrade the sintering conduct of the material. As indicated by Kelvin's condition, a bended fluid surface has an immersed fume pressure a lot more prominent than that of a level fluid surface attributable to the age of extra fluid pressing factor. This further offers a main thrust to vaporous dissemination mass exchange in three-dimensional obstinate frameworks set up by totals and a grid. In this work, as indicated by the above hypothesis, non-oxides, for example, Al4O4C, Al2OC, Zr2Al3C4, and MgAlON fortified Al2O3-based composites were effectively ready at 1873 K in streaming nitrogen utilizing metal Al, plain corundum, and a-Al2O3 miniature powder as the crude materials after an Al-AlN center shell structure was planned at 853 K for 8 hours. The development system of Al2OC is additionally introduced here. Likewise, pitches fortified Al–Al2O3–MgO–ZrO2 composites subsequent to sintering were portrayed and broke down by X-beam diffraction (XRD), examining electron magnifying instrument (SEM) and, energy dispersive spectrometer (EDS), and the impact of the MgO content on the sintered composites was considered.

2. Experimental details

A solid Al2O3 (normal particlesize 60 μm, provider Merck) is utilized for readiness Cr2O3 doped ZTA composite material. Yt triastabilized zirconia (YSZ) particles (normal molecule size1.0 μm, provider Zirox) is added to Al2O3 lattice with a proportion of 90wt% Al2O3/10 wt% YSZ .Samples are combined with 0–1 wt% Cr2O3 (normal molecule size1 μm, provider Sigma Aldrich).The powders are wet blended for 60 minusingultrasonicmachineand30minusingautomatic stirrer subsequently.Themixturesolutionisdriedfor24hin an ovenat200 1C. The powders of Al2O3, YSZ and Cr2O3 are then ball processed for 12 husing 0.8 wt% of polyethyleneglycol 1000 asaplasticizingagent. The morphology of the powders is portrayed through molecule size analyzer. The powder is calcined at600 1C and sintered at 1600 1C for 2h. The X-beam diffraction (XRD) of sintered powder at 1600 1C is read for deciding the level of adjustment of stages [18].

A solid Al2O3 (normal molecule size, 0.5 μm) was utilized as a pattern material. YSZ (GoodFellow Cambrigde Limited) particles (normal molecule size, 1.5 μm) were added to an Al2O3 lattice with a proportion of 80 wt.% Al2O3/20 wt.% YSZ. MgO in normal molecule sizes of 80 nm (Strem Chemicals), 500 nm (Alfa Aesar) and 7000 nm (Alfa Aesar) were added to the Al2O3/YSZ separately. The Al2O3/YSZ tests were ready with various MgO molecule sizes and wt.% going from 0.4 wt.% to 0.9 wt.% for micron size of added substances and 0.4 wt.% to 1.3 wt.% for nano added substances. The powders were then blended utilizing a ball plant for 8 h and squeezed at 295 MPa utilizing a water driven press. The examples were then sintered in a Lenton electric hearth heater at 1600 °C for 4 h with 5 °C/min sintering rate. The machining boundary utilized for this examination. The sintered examples were exposed to nose wear estimations, Vickers hardness (HV30), crack sturdiness and thickness estimation. To compute break strength, the recipe proposed by Niihara for Palmqvist break was utilized [15].

$$3K_{1c}= 0{:}035(Ha^{1/2})(3E/H)^{0.4}(1/a)^{-0:5}$$

Field emission scanning electron microscopy (FESEM) was used to study the microstructure of the sintered samples. The samples were thermally etched in the same furnace used for sintering at 1400 °C for 2 h. Wear analyses were carried out by capturing the images of the cutting tips before and after machining. Images of the insert tip were captured using a high-resolution CCD camera (Model: JAI CV-A1, resolution 1296×1024 pixels) fitted with a 50 mmlens and a 110 mm extension tube. Backlighting was used to highlight the profile of the tool. The field-of-view of the CCD camera is 2.3×2 mm, and the distance from the front end of camera lens to the cutting tool is approximately 60 mm. An algorithm using Wiener filtering, median filtering, morphological operations and thresholding was developed using MatLab to calculate wear area. Detailed processing route, characterization techniques, machining parameter and wear area measurement are described elsewhere [16,17].

3. Results and discussion

3.1. Particle Size, XRD and morphology of MgO nanoparticle

Fig. 1 shows the pictures of the MgO nano-particles utilizing a CM 12 Phillips transmission electron magnifying instrument (TEM). The MgO nano powder utilized for TEM perception was ready as follows. The nanopowder was blended in with liquor and accordingly scattered utilizing a ultrasonic shower for 15 min to stay away from agglomeration. A drop of this scattering was set on a 3 mm distance across copper matrix covered with a carbon film. The copper matrix was analyzed under the TEM with an amplification of 17,000. Every one of the noticed particles showed arbitrary shapes yet with a normal molecule size of 80 nm. Moreover, the MgO nano-particles additionally show square-like morphology, reliable with the perceptions of Seo et al. [18]. Barely any unavoidable agglomerations of MgO nano-particles looking like a micron-sized molecule of MgO were noticed. Fig. 2 shows the XRD diffraction design for all the MgO utilized in this examination. For particles having crystallite estimates under 1000 Å, a widening impact can be seen in the diffraction line. XRD diffraction line for 80 nm MgO (red line) shows expanding impacts to its pinnacles, showing that is have fine molecule size. For 500 nm MgO particles (blue line), the expanding impacts decreased marginally and for 7000 nm particles, sharp pinnacles were noticed.

3.2. Densification and microstructure

Densities of the sintered cutting supplements were estimated utilizing the Archimedes rule. Fig. 3 shows the densities of ZTA–MgO cutting supplements with various MgO molecule sizes. A greatest thickness of 4.31 g/cm3 was gotten by the

example with 80 nm MgO as added substances. An investigation by Lumley and Schaffer [10] showed that by utilizing a coarse molecule as an added substance, it will bring about a profoundly restricted and inadequately disseminated fluid. Along these lines, the effectiveness of the added substance is restricted since it just influences certain spaces of the lattice [10]. Then again, the utilization of fine particles as an added substance will advance the versatility of the fluid during sintering, consequently more spaces of the example will be influenced. Densities acquired utilizing nano-molecule added substances show critical improvement contrasted with added substances in micron size. Nano-particles are prevalently known to have bigger surface regions contrasted with micron particles. Subsequently, tests of ZTA with the expansion of MgO nanoparticles show a vital improvement contrasted with ZTA with the expansion of MgO micron molecule size. Regarding structure, every series of MgO molecule size has a particular piece expected to accomplish the ideal thickness esteem. For tests with 500 nm and 7000 nm MgO as added substances, more than 0.7 wt.% of MgO will deliver ceaselessly diminished qualities which are not critical for conversation. Concerning piece, an investigation led by Azhar et al. [9] and Rittidech et al. [8] likewise showed comparable patterns. Fig. 4 shows the SEM micrographs for ZTA–MgO tests with various estimated added substances. Steady with past examinations [2,9,15,16,19–22], it tends to be seen that the YSZ grains and Al2O3 grains are genuinely circulated among one another. Nonetheless, minor agglomeration is unavoidable.

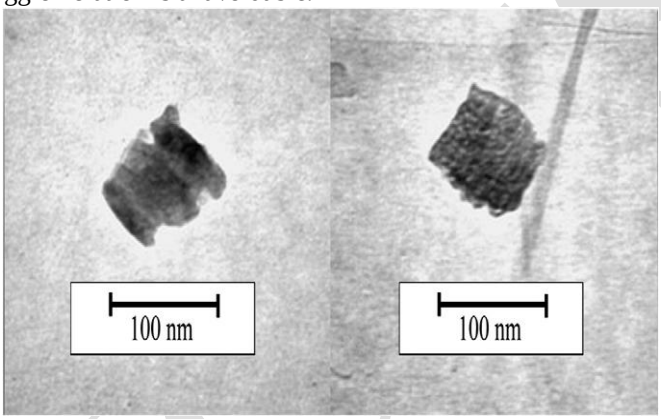

Fig. 1. TEM observations of the MgO nano-powder.

As a general rule, a comparative miniature underlying trademark was seen in these examples for example consistently measured grains with serious level of grain close pressing. Basically no unusual grain development was noticed. Energy dispersive X-beam investigation (EDX) shows that the dull grains are Al2O3 and MgO while the lighter grains are YSZ. For tests with nano-molecule added substances, exceptionally fine white particles were seen on the example surface (Fig. 4b). These nano-particles were seen to be haphazardly dispersed on the example microstructures consequently demonstrating that the MgO didn't agglomerate during the blending cycle.

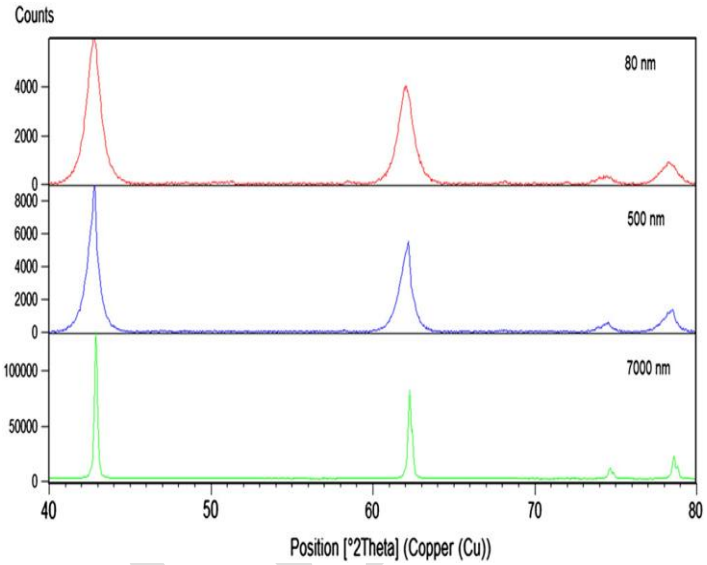

Fig. 2. XRD diffractions for MgO particle sizes.

The effect of the particle size of MgO additives can be seen clearly in the SEM micrographs where Al2O3 grain size with nano-particles of MgO (Fig. 4a) is smaller in size compared to samples with larger MgO sizes (Fig. 4c and d). The observation from the micrographs is consistent with results of density, where higher values of density tend to have closed and smaller packed Al2O3 grains. The characteristic of the close packed Al2O3 grains can be explained by the use of fine particle sized MgO which promotes the mobility of the liquid phase during the sintering process. As a result, more areas of Al2O3 can be affected by the liquid phase, producing uniform and small grain sizes [10]. Samples with 500 nm (Fig. 4(c)) and 7000 nm (Fig. 4(d)) sized MgO showed comparable micrographs, but they also exhibited a few large sized Al2O3 grains and a low level of grain distribution, which is not observed in samples with MgO nano-particles. This might be caused by limited liquid phase mobility during the sintering process as described by Lumley and Schaffer, whereby the use of coarser additives result in a highly localized and poorly distributed liquid [10].

3.3. Vickers hardness and fracture toughness

The impact of MgO molecule size on the Vickers hardness of the cutting addition is displayed in Fig. 5. Vickers hardness increments with better MgO molecule size and progressively diminishes with coarser estimated MgO. The consequence of the hardness esteems is firmly identified with the micrograph perception in Fig. 4, where tests with more modest Al2O3 grain sizes will in general show higher upsides of hardness. The most extreme hardness esteem is acquired with the utilization of 80 nm MgO as added substances for example 1740 Hv. This is because of the little Al2O3 grain size in the example microstructures [23] which came about because of the presence of MgO [7,8]. An investigation directed by Coble uncovered that the job of MgO is to speed up the sintering rate

for Al2O3, subsequently ruining Al2O3 grains from developing.

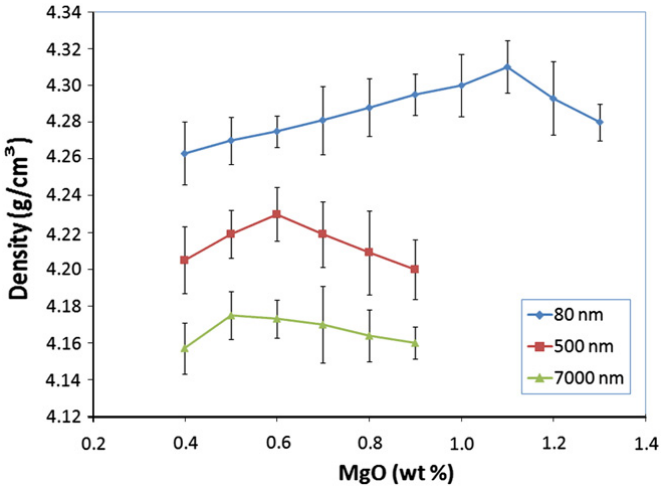

Fig. 3. Results of bulk density for ZTA–MgO cutting inserts with different MgO particle sizes.

The basic condition for Al2O3 to go through spasmodic grain development was turned away by the improvement of the sintering rate by the presence of MgO [7]. It is obviously shown that the impact of MgO molecule size assumes a significant part in the advancement of the hardness worth and microstructures of the examples. This is because of the greater surface space of the fine molecule size of the added substances which would improve the response among Al2O3 and MgO. With bigger molecule measured MgO added substances, the cutting supplements' hardness esteems slowly diminished as the grains of Al2O3 bit by bit become bigger. Indistinguishable from the aftereffects of the thickness tests, the organization expected to accomplish most extreme hardness for every series of molecule size is extraordinary. Reliable with the perception of microstructure and thickness results, tests with the most elevated hardness show shut and more modest stuffed Al2O3 grains and have the most elevated thickness esteem. Indistinguishable with perceptions of thickness, the expansion of more than 0.9 wt.% of micron-sized MgO will deliver consistently diminished qualities that are not critical for a point by point conversation. The impact of MgO molecule size on the crack sturdiness of the cutting addition is displayed in Fig. 6. Break strength diminishes with better MgO molecule size. The aftereffect of crack durability is firmly identified with the micrograph perception in Fig. 4, where tests with more modest Al2O3 grain sizes will in general display lower upsides of crack strength. The most extreme crack strength esteem is gotten with the utilization of 7000 nm MgO as added substances for example 3.62 MPa·m1/2. This is because of the huge Al2O3 grain size in the microstructure displayed in Fig. 4(d). An examination led by Riu et al. clarified that the Al2O3 break durability and imperfection resilience will improve with expanding Al2O3 grain size; because of break spanning by the enormous platelike grains [24]. Thus, tests with more modest Al2O3 grain size will create lower worth of crack durability.

3.4. Wear Region

Pictures of the cutting tips previously, then after the fact machining were caught as displayed in Fig. 7. These two pictures were adjusted naturally before deduction. The product therefore creates pictures displayed in Fig. 5(a) and (b) contingent upon the last state of the supplements. Additionally, the product can precisely ascertain the region contrasts between the two pictures, demonstrated by the dark hued region in Fig. 5(c–d). A bigger dark region shows that the supplements have encountered a more prominent measure of wear, for example more material misfortune has happened due to machining. The slicing embeds were exposed to machine 12.7 mm breadth hardened steel (316L) with profundities of cut 0.8 mm, 0.2 mm/fire up, 40 mm length and 540 rpm of cutting pace without the presence of any cooling fluid. The wear examination in Fig. 8 shows that the cutting additions with 80 nm MgO had the most minimal wear region for example 0.019 mm² on machining hardened steel 316L. The consequence of the wear region investigation connects with the aftereffect of Vickers hardness, which shows that the cutting addition with the most elevated hardness worth will have the most noteworthy wear safe. As per the consequence of Vickers hardness displayed in Fig. 5, the cutting additions with the littlest MgO molecule size has the most elevated Vickers hardness. Subsequently, this cutting supplement shows the most noteworthy wear opposition.

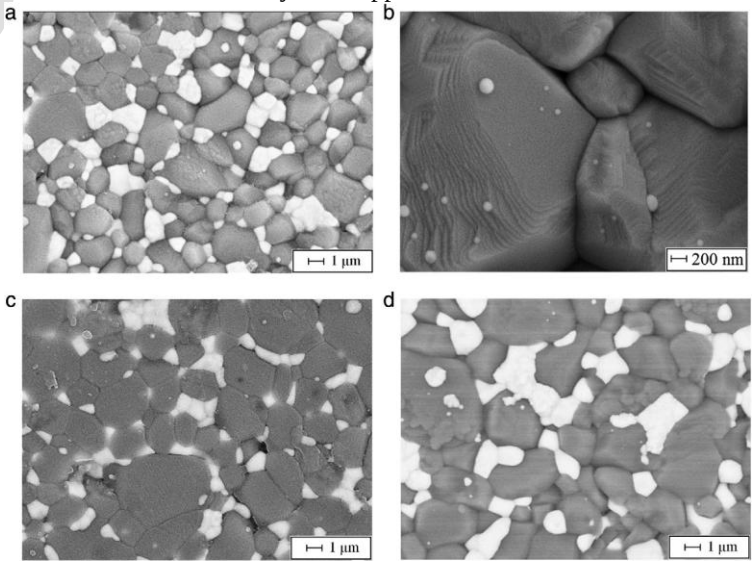

Fig. 4. SEM microstructural images for ZTA–MgO samples; (a) 80 nm MgO, (b) 80 nm MgO with 30,000 magnification, (c) 500 nm MgO and (d) 7000 nm MgO.

Besides, D'Erico et al., [6] likewise expressed that the antiwear execution to a great extent relies upon the hardness of the cutting supplement. Despite the fact that the property of crack durability is significant for cutting supplements in the

metal working application, the wear execution of the ZTA–MgO slicing embeds appear to be not to be influenced by I contrasted with hardness. The impact of MgO piece on ZTA cutting addition wear execution is examined somewhere else [9].

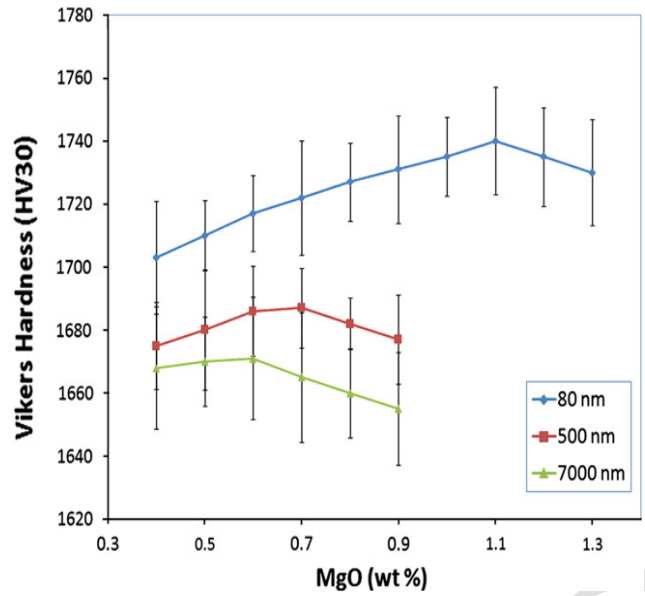

Fig. 5. Vickers hardness of the sintered cutting inserts as a function of MgO wt.% with different particle sizes of MgO.

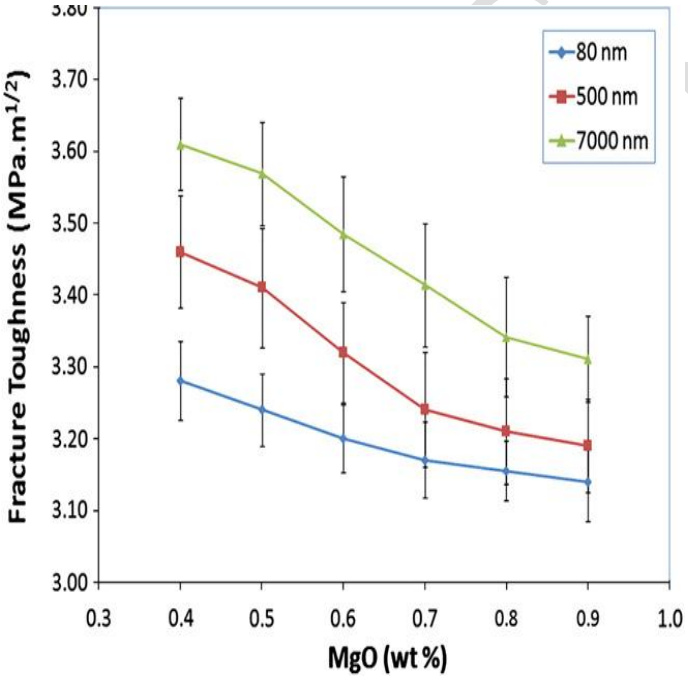

Fig. 6. Fracture toughness of the sintered cutting inserts as a function of MgO wt.% with different particle sizes of MgO.

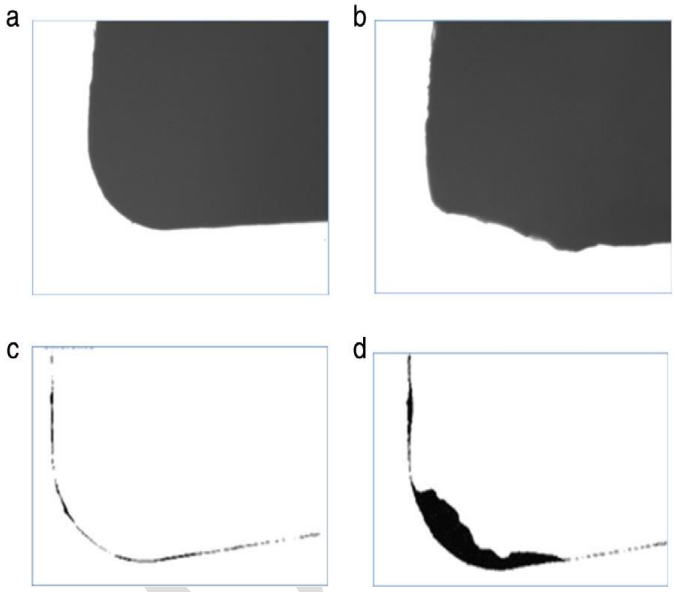

Fig. 7. Images of ZTA–MgO cutting inserts different particle sizes (a) before machining, (b) after machining, (c) 80 nm and (d) 500 nm.

4. Conclusion

The impact of MgO molecule measures on ZTA–MgO cutting supplements was explored in this investigation. It was discovered that expansion of nano added substances fundamentally work on the mechanical and wear execution of the ZTA–MgO cutting additions. Components like miniature underlying highlights, densities and hardness are significant properties that incredibly impact the wear execution of ZTA–MgO cutting supplements. In this manner, a fine MgO molecule size is expected to create thick, high hardness and high wear execution ZTA–MgO artistic cutting additions.

References

[1] Li XS, Low IM. Ceramic cutting tools - an introduction. Key Engineering Materials 1994;96:1–18.
[2] Smuk B, Szutkowska M, Walter J. Alumina ceramics with partially stabilized zirconia for cutting tools. Journal of Materials Processing Technology 2003;133: 195–8.
[3] Lo Casto S, Lo Valvo E, Lucchini E, Maschio S, Piacentini M, Ruisi VF. Ceramic materials wear mechanisms when cutting nickel-based alloys. Wear 1999;225– 229:227–33.
[4] Xu C, Ai X, Huang C. Fabrication and performance of an advanced ceramic tool material. Wear 2001;249:503–8.
[5] Senthil Kumar A, Raja Durai A, Sornakumar T. Development of yttria and ceria toughened alumina composite for cutting tool application. International Journal of Refractory Metals & Hard Materials 2007;25:214–9.
[6] D'Errico GE, Bugliosi S, Calzavarini R, Cuppini D. Wear of advanced ceramics for tool materials. Wear 1999;225–229:267–72.
[7] Coble RL. Sintering crystalline solids. II. Experimental test of diffusion models in powder compacts. Journal of Applied Physics 1961;32:793–9.

[8] Rittidech A, Portia L, Bongkarn T. The relationship between microstructure and mechanical properties of Al2O3–MgO ceramics. Materials Science and Engineering A 2006;438–440:395–8.
[9] Azhar AZA, Mohamed H, Ratnam MM, Ahmad ZA. The effects of MgO addition on microstructure, mechanical properties and wear performance of zirconia-toughened alumina cutting inserts. Journal of Alloy and Compunds 2010;497:316–20.
[10] Lumley RN, Schaffer GB. The effect of additive particle size on the mechanical properties of sintered aluminium–copper alloys. Scripta Materialia 1998;39: 1089–94.
[11] Fu CT, Wu JM, Li AK. Microstructure and mechanical properties of Cr3C2 particulate reinforced Al2O3 matrix composites. Journal of Materials Science 1994;29:2671–7.
[12] Jeong YK, Niihara K. Microstructure and mechanical properties of pressureless sintered Al2O3/Sic nanocomposites. Nanostructured Materials 1997;9:193–6.
[13] Ji Y, Yeomans JA. Processing and mechanical properties of Al2O3-5 vol.% Cr nanocomposites. Journal of the European Ceramic Society 2002;22:1927–36.
[14] Nawa M, Nakamoto S, Sekino T, Niihara K. Tough and strong Ce–TZP/Alumina nanocomposites doped with titania. Ceramics International 1998;24:497–506.
[15] Magnani G, Brillante A. Effect of the composition and sintering process on mechanical properties and residual stresses in zirconia–alumina composites. Journal of the European Ceramic Society 2005;25:3383–92.
[16] Azhar AZA, Ratnam MM, Ahmad ZA. Effect of Al2O3/YSZ microstructures on wear and mechanical properties of cutting inserts. Journal of Alloys and Compounds 2009;478:608–14.
[17] Shahabi H, Ratnam M. On-line monitoring of tool wear in turning operation in the presence of tool misalignment. The International Journal of Advanced Manufacturing Technology 2008;38:718–27.
[18] Seo DJ, Bin Park S, Chan Kang Y, Leong Choy K. Formation of ZnO, MgO and NiO nanoparticles from aqueous droplets in flame reactor. Journal of Nanoparticle Research 2003;5:199–210.
[19] Sadangi RK, Shukla V, Kear BH. Processing and properties of ZrO2(3Y2O3)-Al2O3 nanocomposites. International Journal of Refractory Metals and Hard Materials 2005;23:363–8.
[20] Hao JKC, Azhar AZA, Ratnam MM, Ahmad ZA. Wear performance and mechanical properties of 80 wt% Al2O3/20 wt% YSZ cutting inserts at different sintering rates and soaking times. Materials Science and Technology 2010;26:95–103.
[21] Basu B, Vleugels J, Van Der Biest O. ZrO2–Al2O3 composites with tailored toughness. Journal of Alloys and Compounds 2004;372:278–84.
[22] Lee DY, KimD-J, KimB-Y. Influence of alumina particle size on fracture toughness of (Y, Nb)-TZP/Al2O3 composites. Journal of the European Ceramic Society 2002;22:2173–9.
[23] Tajima K, Hwang HJ, Sando M, Niihara K. PZT nanocomposites reinforced by small amount of oxides. Journal of the European Ceramic Society 1999;19:1179–82.
[24] Riu D-H, Kong Y-M, Kim H-E. Effect of Cr2O3 addition on microstructural evolution and mechanical properties of Al2O3. Journal of the European Ceramic Society 2000;20:1475–81.